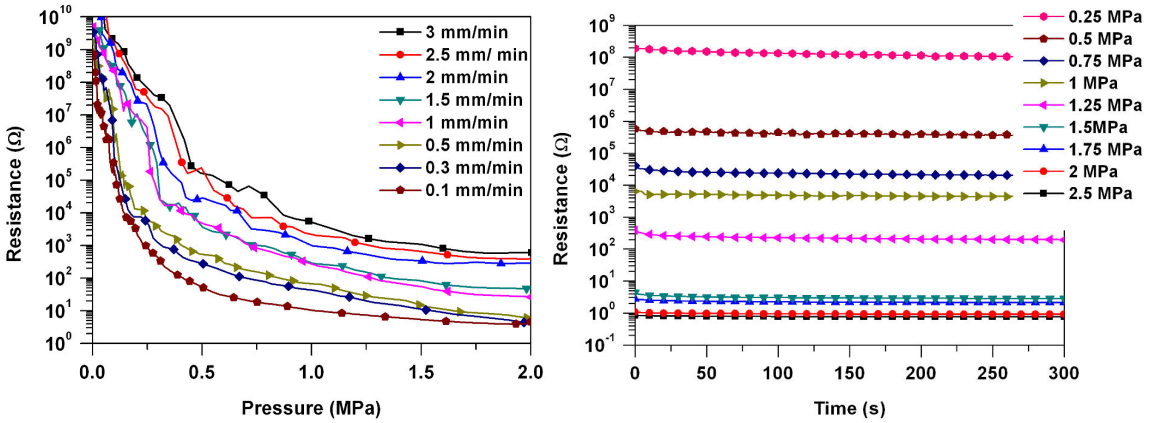

Figure 3.8. (a) Electrical resistance of PDMS-Ni composite as a function of the applied compression rate and (b) time variation of PDMS-Ni composite resistance under different uniaxial applied pressures.

thick sample with a 10:1 PDMS composition and nickel content of 500 phr.

Reusability of the material and repeatability of the measurements are fundamental if the composite should be used for sensor applications. Therefore it was tested how the electrical resistance of the samples varies during ten cycles of compression and decompression from 0 to 2 MPa. Fig.3.9(a) reports the values of resistance obtained at the maximum compression reached during every cycle from a 2 mm thick sample with a 10:1 PDMS composition and nickel content of 500 phr, while Fig.3.9(b) shows the complete variation during all cycles. The elastic behaviour of the material allows the composite to completely recover the initial form and particles arrangement after every cycle, restoring the resistance value for the insulating state. In contrast the maximum compression value shows some variation during the whole measurement, there is a slight increase probably due to hysteresis phenomena during the compression and decompression cycles. The four curves in Fig.3.9(a) evidence how the effect of material creep increases raising the compression velocity and that faster rates result in higher values of resistance when the composite is compressed, as already reported in Fig.3.8(a).

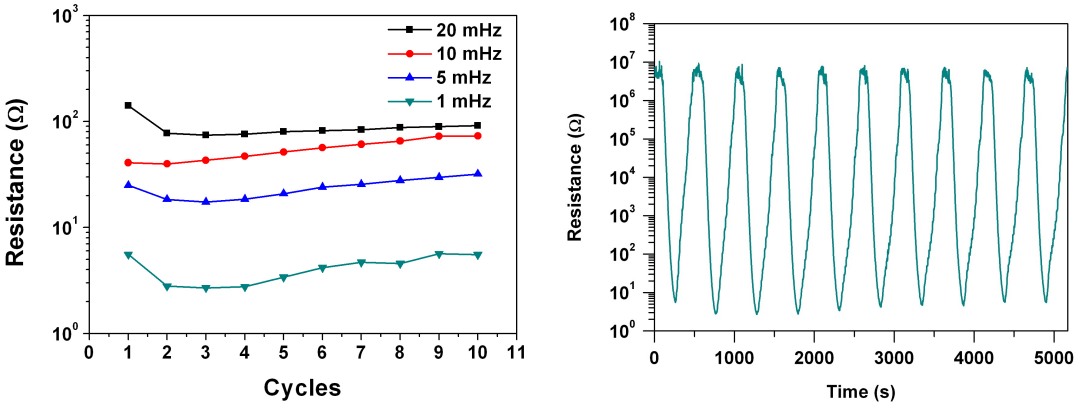

(a) (b)

Figure 3.9. (a) Maximum resistance values of PDMS-Ni sample obtained for 10 cycles of compression and decompression at different compression rate and (b) time variation of the electrical resistance of PDMS-Ni composite during 10 cycles of compression and decompression at a velocity of 0.2 mm/min (1 mHz).

3.5 Comparison of experimental and simulated piezoresistive response

A detailed analysis of the pressure sensitivity dependence of the PDMS-Ni composite on composition, shape and dimension allowed a selection of the best configuration for pressure sensor application. The composite with nickel content of 500 phr and PDMS copolymer-curing agent 10:1 was selected to achieve the best compromise between piezoresistive response and easiness in the fabrication process. The metallic filler amount corresponds to the 50% of the total volume and thus the material maintains a high deformability, even if the quantity of metal particles is elevated. In contrast the 550 phr composites were stiffer and difficult to prepare because of the high metal volume.

In order to compare the experimental functional response under compressive pressure with the theoretical model elaborated from those proposed by Zhang [7] and Lantada [8], samples with a footprint of 10x10 mm^2 and a thickness of 1 mm were prepared. All the prepared composites presented an insulating behaviour in the uncompressed state with a value higher than 1 GΩ confirming the absence of conductive paths. While under compression the resistance strongly decreased even below 1 Ω for pressure up to 2 MPa. Functional characterization of a sample with an initial value of 14 GΩ and a variation of resistance up to 9

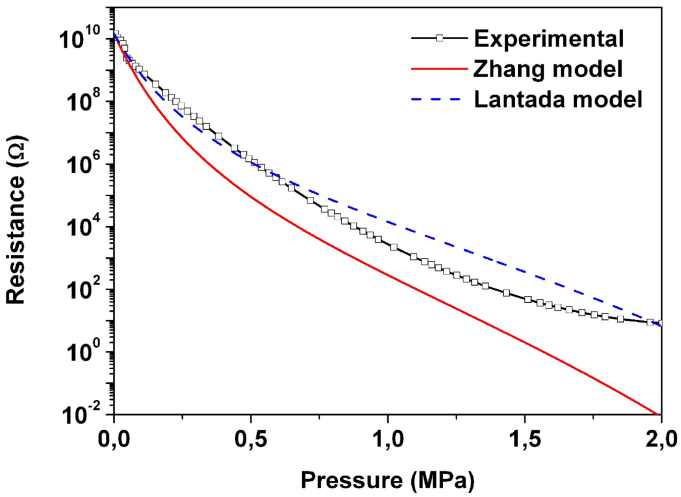

Figure 3.10. Comparison between the experimental and theoretical values of the electrical resistance of PDMS-Ni composite as function of compressive pressure. The theoretical values were obtained from equations (2.17) and (2.19), corresponding to Zhang and Lantada models respectively.

orders of magnitude are shown in Fig.3.10. In the same graph the resistance values obtained experimentally are compared with the data obtained from the simulation performed with equations (2.17) and (2.19). Both the models agree with the experimental data, especially with the one proposed by Lantada, which contains less approximations with respect to the Zhang's model. The trend confirms that the conduction mechanism is based on quantum tunnelling effect. Some deviations, in particular at higher compression, can be observed and attributed to the approximation used for the computation of the interparticle distance without mechanical deformation. In fact, the nickel particles have a spread distribution of dimension and their shape is not spherical, but presents a highly irregular surface. Moreover, slight variations of this parameter induce large changes in the results obtained from both the models.

Similarly sheets of PDMS-Ni composite with 1 mm thickness, 6 mm width, and a length of 40 mm were used for the piezoresistive analysis under tensile pressures. The samples presented again an insulating behaviour in the undeformed state ($>$100 GΩ) and experienced a decrease of electrical resistance of almost 10 orders of magnitude over a pressure range of 2.5 MPa, even if the larger variation was registered before 0.5 MPa. The comparison between the experimental data and the values obtained from the proposed theoretical model are shown in Fig.3.11. At low pressures there is a good agreement between the experimental

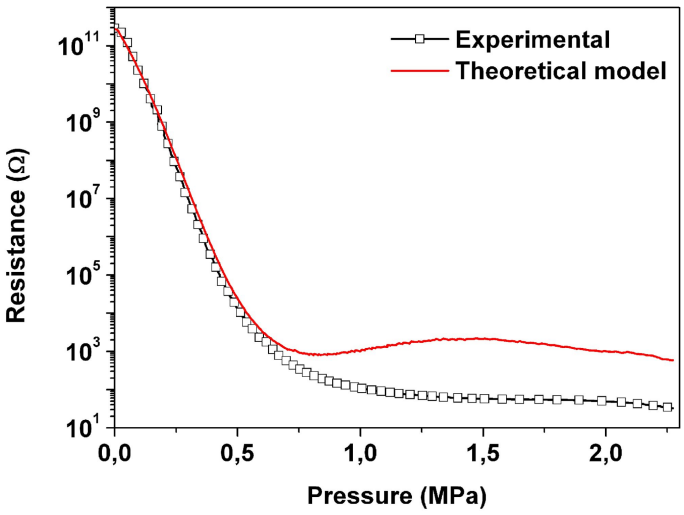

Figure 3.11. Comparison between experimental and theoretical values of the electrical resistance of PDMS-Ni composite as function of tensile pressure. The theoretical values were obtained from equation (2.25).

and the theoretical values obtained from equation (2.25). Upon increasing the tensile stress, the discrepancy between the two curves increases. This effect is mostly due to a change in the mechanical behaviour of the composite. Since the theoretical model depends on empirical parameters, such as Young's Modulus, the trend of the materials stiffness affect the model prediction. Indeed a minimum in the tensile modulus vs. pressure curve at 1.5 MPa causes an increase in the value of the electrical resistance computed with the theoretical model at the corresponding pressure. On the contrary this trend was not observed in the experimental measurement.

3.6 Mechanical characterizations

The mechanical properties of PDMS-Ni composite (500 phr) were tested and compared with the values obtained from samples of pure polymer. Some fundamental figures of merit are reported in Tab.3.2. The dimensions of the samples were chosen according to the specific mechanical characterization measurements. The "dog bone" samples for tensile modulus analysis were prepared in accordance with the UNI 6065:2001 standard. The samples used for compressive modulus analysis were prepared with a square footprint of 10x10 mm^2 and

a thickness of 1 mm in accordance with UNI ISO 7743:2008 standard.

Determining the mechanical performance is fundamental not only for structural materials, but also for functional ones and for their integration into more complex systems i.e. sensors and smart devices. For example in tactile sensors the knowledge of the mechanical properties of the functional material is crucial for the design of electrodes, for the mechanical coupling with the support material and for the interaction with the environment and other components.

From the mechanical point of view, the most important aspect of elastomeric reinforcement is the nature of the bonding between the filler particles and the polymer chains [9]. One factor which is directly related to the adsorption of polymer chains onto filler surfaces are changes in the distribution of end-to-end vectors of the chains. The volume taken up by the filler particles causes related changes in the mechanical properties of the polymer host matrix. An effect of the particle presence is the increase of the dimensions of the polymeric chains when the filler particles are smaller with respect to the dimensions of the network chains. On the other hand, particles that are relatively large tend to reduce the chain dimensions [10].

The filler size is only one of several parameters affecting the overall mechanical characteristics of a composite system. The filler type, shape and amount, as well as the efficient coupling of fillers and polymer matrix, strongly influence the mechanical properties of the composites. Physical quantities such as compressive or flexural strength, hardness and Young's modulus improve as the filler content increases. At the same time the polymerization shrinkage decreases. However, in some cases an optimum value can be achieved at a certain filler volume-fraction and then declines upon any further increase of the volume filler fraction [11]. Several empirical or semi-empirical equations have been proposed to predict

SAMPLE	**PDMS**	**PDMS-Ni**
Tensile modulus (MPa)	1.64 ± 0.05	8.34 ± 0.82
Ultimate tensile strength (MPa)	4.45 ± 0.42	3.19 ± 0.84
Ultimate tensile deformation (%)	146 ± 8	26 ± 4
Compressive modulus at 10% (MPa)	1.48 ± 0.24	6.18 ± 1.07
Compressive modulus at 20% (MPa)	1.56 ± 0.13	8.83 ± 1.61
Dynamic modulus (MPa)	2.99	28.98

Table 3.2. Mechanical properties of PDMS-Ni composite and pure PDMS samples.

the mechanical properties of polymer composite materials [11].

In the composite samples of the present work, where the particle filler aspect ratio is small, such as for spherical particles, the elastic modulus depends on the modulus of the components and on the particle loading. Therefore the measured composite moduli are enhanced by adding particles to the elastomeric matrix since the modulus of Nickel particles is much higher than the PDMS matrix one.

The Young's modulus is the stiffness (the ratio between stress and strain) of a material at the elastic stage of a tensile/compressive test. Since Young's modulus is measured at relatively low deformation (as suggested by UNI ISO 7743:2008 in correspondence to 10 and 20 percent of compressive deformation) there is insufficient deformation to cause interface separation. Thus, the interface adhesion between the nickel filler particles and PDMS polymer matrix does not conspicuously affect the elastic modulus.

Otherwise, ultimate tensile strength (defined as the maximum stress that the material can sustain under uniaxial tensile loading) strongly depends on the stress transferred between the particles and the matrix. For well-bonded particles, the applied stress can be efficiently transmitted from the matrix to the particles. However, for poorly bonded microparticles, strength reduction occurs by increasing the filler amount [11].

Although the high surface area of spiky nickel particles guarantees an efficient stress transfer mechanism, in Tab.3.2 is possible to observe a slight reduction of the composite ultimate tensile strength value in respect to the pure PMDS one and a relative marked reduction of the corresponding ultimate deformation at break.

3.7 Electrical characterization

Current-voltage measurements were carried out on the PDMS-Ni composite in order to investigate the more suitable voltage range to be used for sensor applications. The composite presented non-linear characteristics strongly dependent on the applied voltage and on the deformation. The graphs in Fig.3.12 show the current-voltage characteristics measured from -20 V to 20 V at different compressive pressures. At low applied pressure, the current has an exponential trend that is typical of a tunnel barrier [12].

Upon increasing the deformation, the current is expected to increase because of the reduction in the interparticle distance and still having an exponential dependence on the

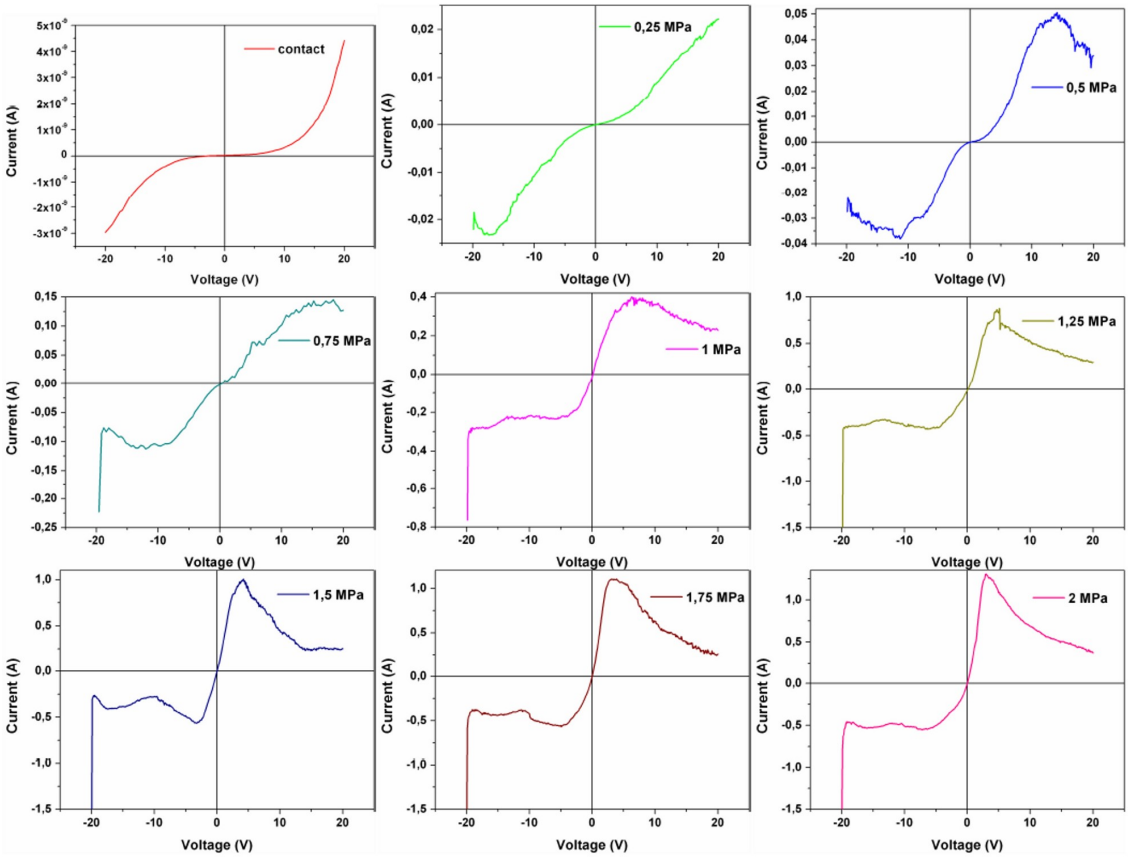

Figure 3.12. Current-voltage characteristics between -20 and 20V at different applied compressive pressures from 0 to 2 MPa.

voltage. In contrast after a certain voltage value the current decreases, until inverting the behaviour and obtaining a negative slope. The current inversion point moves to low voltages while increasing the compressive pressure on the samples and hence the conductivity. Fig.3.13 shows a current inversion point variation from 18 V to 3 V while increasing the pressure from 0.75 MPa to 2 MPa. This phenomenon could be attributed to an accumulation of charges on the surface of the metal particles. The electrons cannot tunnel in the direction of the current flow, because of larger gaps, thus they are accumulated on the particles and cause an increase in the local electric field [1]. This enhancement induces a rising in the height of adjacent potential barriers thus decreasing the conductivity of the sample. The negative slope in the I-V curve is reached when a sufficient number of tunnel gaps (therefore also the tunnelling paths along the samples) are blocked to compensate the increase in the

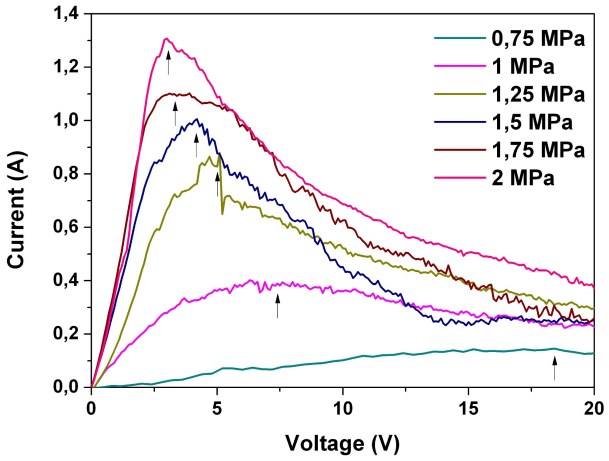

Figure 3.13. Current-voltage characteristics between 0 and 20 V at different applied compressive pressures from 0.75 MPa to 2 MPa. The current inversion point of each curve is showed by the arrow.

tunnelling probability with the corresponding voltage. The current has to be necessarily high to inject enough trapped charges in the sample and to maintain or increase them.

The current-voltage characteristics also showed a dependence on the initial voltage value. This behaviour was observed by applying an increasing voltage ramp to the sample and then a decreasing one, as shown in Fig.3.14. The plotted curves, collected from -20 V and 20 V and from 20 V and -20 V on a sample compressed by a pressure of 1.5 MPa, are symmetric with respect to the origin. At the beginning of the measurement, the current flowing in the sample is very high (above 1.5 A which is the limitation of the instrument), but it instantaneously decreases because of the trapping charge phenomenon. Upon reducing the voltage (in absolute value) the effect of the charges decreases till the exponentially trend of the current is restored. Moving beyond the zero voltage, the current continues to rise by increasing the electric field, until the distribution of charges on the surface of the particles is restored. The value of the current (and therefore the voltage value) corresponding to these charging phenomena are higher than the discharging ones.

The basic unit of this composite material is the tunnel junction composed by the insulating dielectric material, the PDMS, placed between two electrical conductors, the metal particles. Then a capacitance value can be attributed to the barrier, depending on the distance between the particles, the cross sectional area of tunnelling and the dielectric constant

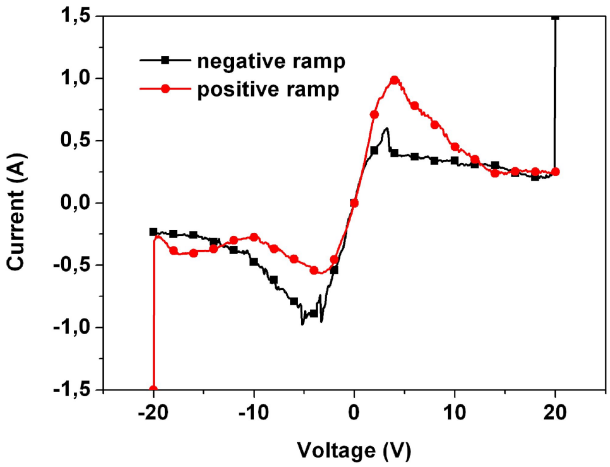

Figure 3.14. Current-voltage characteristics between -20 V and 20 V obtained with positive and negative voltage ramps. The applied constant pressure on the samples was 1.5 MPa.

of the polymer. Since the composite sample is constituted by a countless number of tunnelling junctions, it can be modeled as a circuit composed by a parallel of a variable resistor and a variable capacitor both dependent on the applied pressure. To confirm this model the equivalent circuit of the composite was characterized by applying a triangular voltage waveform signal with peak amplitude of 25 V at different frequencies and with various compressive loads. In the case of samples simply in contact with the electrodes (pressure below 10 kPa), at low frequencies the current followed an exponential trend, showing the resistive behaviour of the composite material (i.e. in the equivalent circuit the current flowing mostly in the resistor). Upon increasing the frequency, the contribution of the capacitance became more and more important till completely covering the effect of the resistor at 100 Hz by returning a square wave as current signal (current flowing in the capacitor). By compressing the sample, the contribution of the capacitance decreased and the resistance behaviour got even more predominant, because the decreasing of the interparticle gap increases the tunnelling current. Evidences of this phenomenon are shown in Fig.3.15. The plotted current signals were obtained by applying a triangular waveform to the samples at 100 Hz and 1 kHz and varying the pressure up to 0.25 MPa. Above this compression the capacitance contribution was not significantly appreciable.

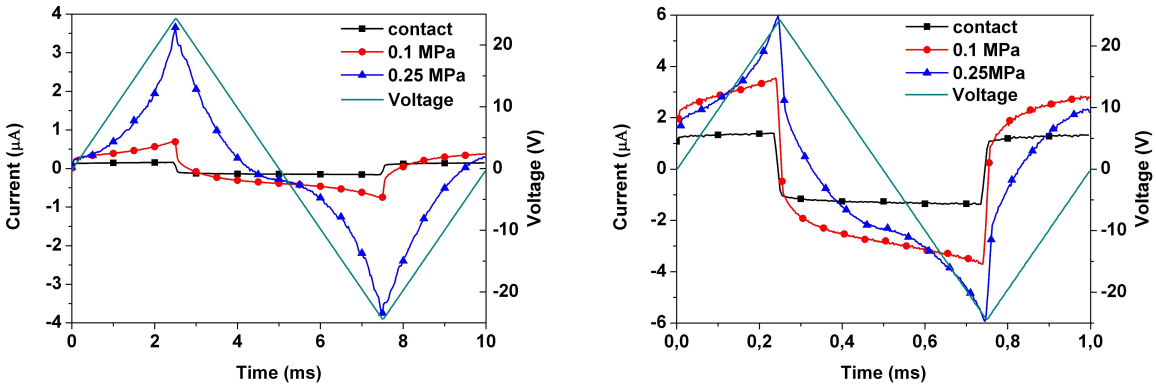

Figure 3.15. Current-voltage characteristics for different applied compressive pressures obtained with a triangular voltage signal at a) 100 Hz and b) 1 kHz.

3.8 Electrical and functional response at different temperature

Thermal expansion is a prominent effect in elastomeric polymers [13]. Dow Corning declares a linear thermal coefficient for Sylgard 184 as high as $3.1\text{x}10^{-4}\text{K}^{-1}$. The influence of the temperature on the PDMS-Ni composite is directly linked to the interparticle separation. By increasing the temperature, the insulating layer between the metal particles expands and the probability of tunnelling decreases. The nickel particles also suffer from thermal expansion when heated up, but the effect is too small compared to the PDMS one that it can be neglected. Evidence of this phenomenon can be observed in Fig.3.16. For these I-V measurements the temperature was varied from 50 °C up to 175 °C keeping the compressive pressure on the sample constant at 0.75 MPa. Similarity can be found between these graphs and the current-voltage characteristics as function of applied pressure presented in Fig.3.12 since both the temperature and pressure modify the thickness of the PDMS layer. Indeed an increase in temperature modifies the I-V characteristics in the same way as a decrease in the sample compression.

Since there is a temperature dependence in the I-V characteristic even the piezoresistive behaviour of the composite material is subjected to changes. The analysis was performed by evaluating the electrical resistance of the composite varying the uniaxial pressure from 0 to 2 MPa. The measurement was repeated at different temperatures, ranging from 25 °C

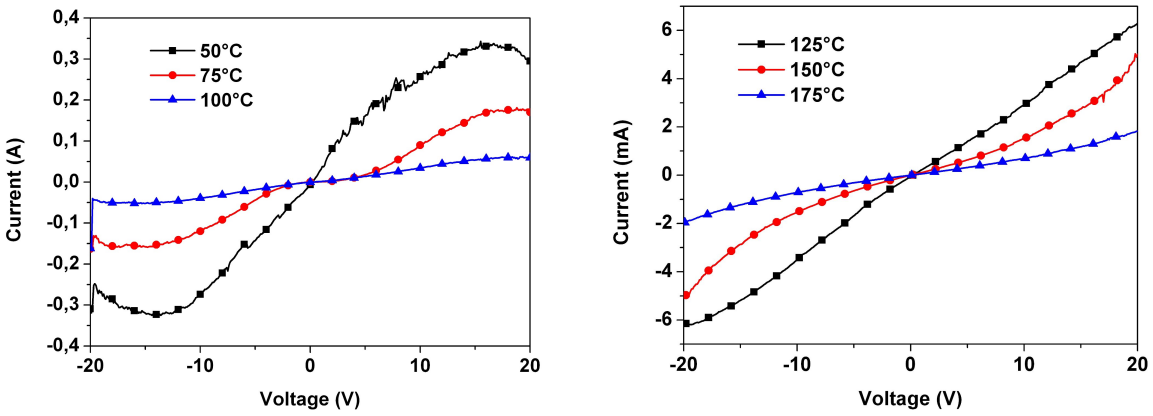

Figure 3.16. Current-voltage characteristics at different temperatures for a fixed applied compressive pressure of 0.75 MPa.

to 175 °C with a step of 25 °C. Fig.3.17 shows the values of electrical resistance plotted as a function of the temperature for fixed pressures of 0.5, 1, 1.5 and 2 MPa. As expected the materials shows a PTC (Positive Temperature Coefficient) effect or rather the resistance of the composite is increasing exponentially heating up the samples, according to the tunnelling mechanism of conduction.

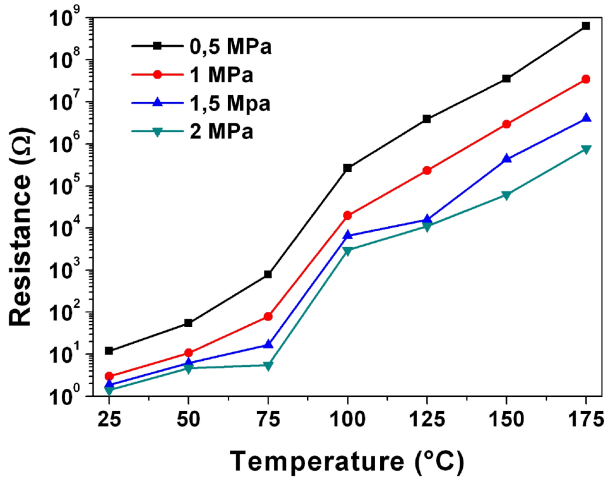

Figure 3.17. Electrical resistance as function of temperature and uniaxial pressure.

Bibliography

[1] D. Bloor, K. Donnelly, P. J Hands, P. Laughlin, and D. Lussey. A metal-polymer composite with unusual properties. *J. Phys. D: Appl. Phys.*, 38:2851–2860, 2005.

[2] M.K. Abyaneh and S.K. Kulkarni. Giant piezoresistive response in zinc-polydimethylsiloxane composites under uniaxial pressure. *J. Phys. D: Appl. Phys.*, 41:135405, 2008.

[3] G. Ausanio, A.C. Barone, C. Campana, V. Iannotti, C. Luponio, G.P. Pepe, and L. Lanotte. Giant resistivity change induced by strain in a composite of conducting particles in an elastomer matrix. *Sensors and Actuators A: Physical*, 127(1):56–62, 2006.

[4] K.S. Chou, K.C. Huang, and Z.H. Shih. Effect of mixing process on electromagnetic interference shielding effectiveness of nickel/acrylonitrile-butadiene-styrene composites. *Journal of Applied Polymer Science*, 97(1):128–135, 2005.

[5] C.J. Edgcombe and U. Valdrè. Microscopy and computational modelling to elucidate the enhancement factor for field electron emitters. *Journal of Microscopy*, 203:188–194, 2001.

[6] F.M. Sasoglu, A.J. Bohl, and B.E. Layton. Design and microfabrication of a high-aspect-ratio PDMS microbeam array for parallel nanonewton force measurement and protein printing. *Journal of Micromechanics and Microengineering*, 17(3):623–632, 2007.

[7] X.W. Zhang, P.Y. Zheng, and X.Q. Yi. Time dependence of piezoresistance for the conductor-filled polymer composites. *J Polym Sci Part B: Polym Phys*, 38(21):2739–2749, 2000.

[8] A.D. Lantada, P. Lafont, J.L.M. Sanz, J.M. Munoz-Guijosa, and J.E. Otero. Quantum tunnelling composites: Characterisation and modelling to promote their applications as sensors. *Sensors and Actuators A: Physical*, 164(1-2):46–57, 2010.

[9] J.E. Mark, R.A. Hussaein, T.Z. Sen, and A. Kloczkowski. Some simulations on filler reinforcement in elastomers. *Polymer*, 46(21):8894–8904, 2005.

[10] D.R. Paul and J.E. Mark. Fillers for polysiloxane ("silicone") elastomers. *Progress in Polymer Science*, 35(7):893–901, 2010.

[11] S.Y. Fu, X.Q. Feng, B. Lauke, and Y.W. Mai. Effects of particle size, particle/matrix interface adhesion and particle loading on mechanical properties of particulate-polymer composites. *Composites Part B: Engineering*, 39(6):933–961, 2008.

[12] W.F. Brinkman, R.C. Dynes, and J.M. Rowell. Tunneling conductance of asymmetrical barriers. *Journal of Applied Physics*, 41(5):1915–1921, 1970.

[13] H.S. Chuang and S. Wereley. Design, fabrication and characterization of a conducting PDMS for microheaters and temperature sensors. *Journal of Micromechanics and Microengineering*, 19(4), 2009.

Chapter 4

An innovative PDMS-copper piezoresitive composite for flexible tactile sensor

In this chapter is presented the preparation and characterization of composite material based on multi branched spiky copper particles dispersed into silicone matrix for piezoresistive tactile sensor application. The material showed giant variation of electrical resistance under the application of both compressive and tensile forces with a sensitivity tunable with variation on the process parameter as filler amount and sample thickness. This phenomenon is promoted by the characteristic shape of the particles, presenting multi-branched microstructures covered by very sharp nanometric spikes on the surface. Furthermore this morphology helps the polymer to intimately coat the filler, avoiding physical contact between close particles and resulting in an insulating electric behavior when no mechanical deformation is applied to the specimens. When the samples are subject to a compressive strain, the gap represented by the insulating layer between the metal particles is reduced, thus causing an exponential increase of the probability for the electrons to tunnel between neighbouring particles. As a consequence, the electrical conduction of the specimens increases of several orders of magnitude. In contrast under the application of a tensile stress, the gaps between the particles in the direction parallel to the force increases, while the interparticle layers on the perpendicular axes are reduced guaranteeing a decreasing of the whole electrical resistance of the sample.

4.1 Preparation of the composite

The copper powder used for this work was supplied by Pometon Ltd. (Type LT10). The synthesis process is similar to the one employed for the preparation of the nickel-based composite. The functional material was prepared by dispersing the conductive particles in the PDMS copolymer and gently mixing at room temperature, in order to avoid the disruption of the tips at the particle surface. Then the PDMS curing agent was added to the blend and the obtained paste was then mixed manually again, poured in Poly(methyl methacrylate) (PMMA) moulds, fabricated by milling techniques, and outgassed under vacuum for 1 hour at room temperature. After all the air bubbles were eliminated, the mould was clamped between two PMMA plates in order to obtain flat surfaces and the composite was thermally cured at 75 °C for three hours.

Tab.4.1 reports the combinations of thickness and filler amount exploited for the PDMS-Cu composite. The quantity of copper particles ranges from 150 to 250 parts per hundred resin (phr), because lower quantities do not exhibit piezoresistive properties in the investigated pressure range, while highly filled composites were difficult to process and cure.

The PDMS composition investigated was only the 10:1 copolymer-curing agent weight ratio, because on the basis of the observation reported in chapter 3 on nickel-silicone composites it guarantees an optimum stiffness for the sensitivities requested in tactile applications. In fact the mobility of the copper particles inside the elastomeric matrix directly affects the piezoresistive behaviour of the composite. The probability of tunnelling of the electrons increases when the insulating polymeric layer placed between two closed particles is deformed and thinned by the external load. Since we used a bi-component PDMS, the Young's modulus of the obtained composite can be tuned by varying the copolymer-curing agent ratio [1]. Then the sensitivity of the final material to the applied pressure would be lower for compositions with a higher content of PDMS curing agent with respect to the reference value (10:1 PDMS copolymer:PDMS curing agent), since a more cross-linked polymer with higher stiffness would be obtained [2].

This effect is further enhanced in composites with a lower content of copper particles, because the thickness of the polymeric layer among metal particles increases.

Thickness	Copper content
0.5 mm	150, 200, 250 phr
1 mm	150, 200, 250 phr
2 mm	150, 200, 250 phr

Table 4.1. Variation of process parameters for the preparation of PDMS-Cu composite samples

4.2 Structural and morphological analysis

FESEM micrographs acquired on the as-received copper powder showed particles in the range of 10-20 μm, having a highly irregular surface. The particles present multi-branched microstructures covered by very sharp spikes (up to a few micrometers in length), as shown in Fig.4.1.

FESEM characterizations on the cured composite showed that the mechanical mixing step assures a uniform distribution of the metal particles inside the polymer matrix, avoiding the formation of large aggregates and without significantly changing the surface roughness (Fig.4.2). Every conductive filler is uniformly and completely coated by the polymer that follows the particle morphology (as shown by the trace of a copper particle in Fig.4.2(a) removed during the cutting in the FESEM preparation). In this way closer particles do not touch each other guaranteeing an insulating behaviour (100s of MΩ up to some GΩ) in its undeformed state even if the metallic loading is elevate (around 50% in volume).

4.3 Functional characterization under compressive pressure

As similarly reported for nickel-based composite, the functional properties of PDMS-Cu composite are also strongly dependent on the PDMS composition (as already described in section 4.1), on the metal filler content and on the sample final thickness.

Since the functional material is composed by a metal part and a polymer one, the variation of their mutual concentrations tunes the composite piezoresistive response, consequently modifying the sensitivity of the final sensor. Higher metallic filler quantity leads to a higher pressure sensitivity since the tunnelling gap between neighbouring particles in the undeformed state is smaller than in composites with a lower metallic content (i.e. decrease the thickness of the potential barrier). This gap is further reduced when the sample is compressed. An example of the functional response of the PDMS-Cu is shown in Fig.4.3 for

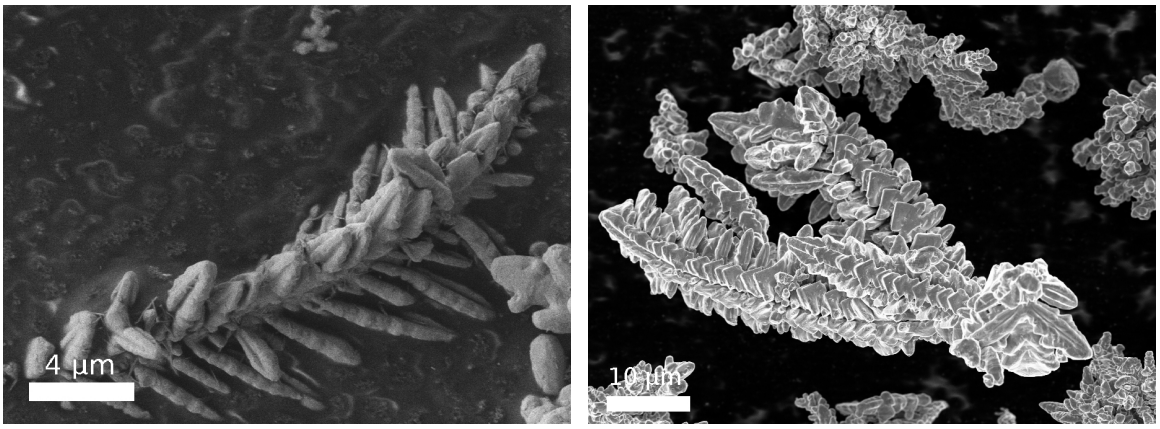

(a) (b)

Figure 4.1. FESEM images of copper powder at different magnifications. The scale bars correspond to (a) 4 and (b) 10 μm

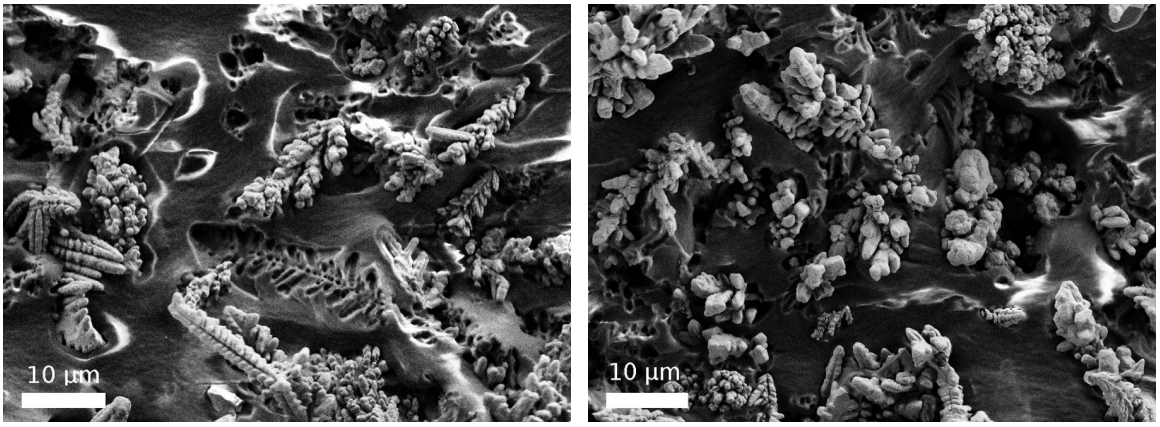

(a) (b)

Figure 4.2. FESEM images of PDMS-Cu composite. The scale bars correspond to 10 μm

samples with a thickness of 1 mm. All the compositions exhibit an insulating behaviour without any applied load. The electrical resistance of the undeformed sample is higher than 100 MΩ, confirming that the copper particles are completely covered by the polymer, as already observed with FESEM analysis, and there are no conductive paths inside the composite.

Under the application of a compressive pressure the resistance of the samples decreases of several orders of magnitude. At 2 MPa the sample of 250 phr suffers a variation of around

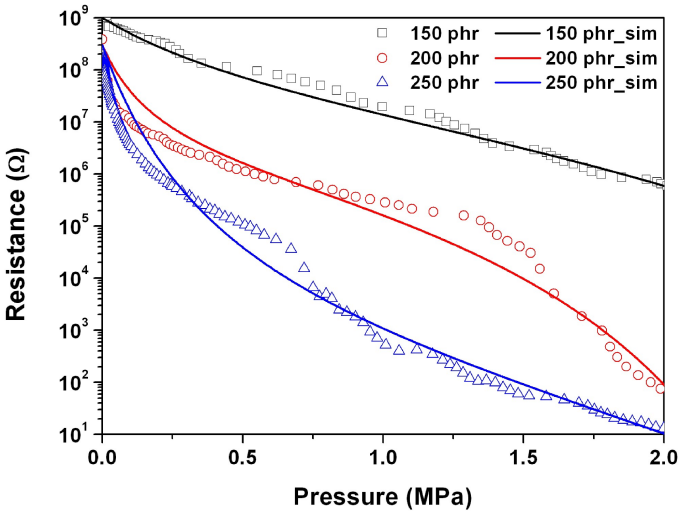

Figure 4.3. Comparison between the experimental and theoretical values of the electrical resistance of PDMS-Cu composite as function of compressive pressure and of copper particles content. The theoretical values were obtained from equation (2.19), corresponding Lantada model.

eight orders of magnitude while the 200 phr composition of seven orders and the 150 phr of just three. The comparison of the functional response of the different composites with the behaviour computed with equation (2.19), reveals that the theoretical model well predicts the piezoresistive response of the material for all the range of applied pressure.

As already stated in chapter 2 piezoresistive materials can be analyzed and compared by evaluating their piezosensitivity and strain sensitivity. For the composite presented in Fig.4.3 the calculated piezosensitivity was 0.0109/kPa for the 250 phr sample, 0.0061/kPa for the 200 phr and 0.0037/kPa for the 150 phr one. These values are in line with piezoresistive composites made with PDMS or epoxy resin using nickel particles as filler [3, 4]. The strain sensitivity (gauge factor) values calculated for the 250 phr, the 200 phr and the 150 phr samples were 48, 42 and 27, respectively. These gauge factors are higher than the values found for polymer composites prepared with zinc particles or other copper particles (∼30 or lower) [5, 6], but lower than those found for nickel based composites (∼200) [3, 6], where the metal content is higher. The correlation between piezosensitivity and gauge factor is the elastic modulus of the functional material, hence a composite with low gauge factor could have a high piezosensitivity that is more interesting for our purpose of fabricating a tactile sensor array.

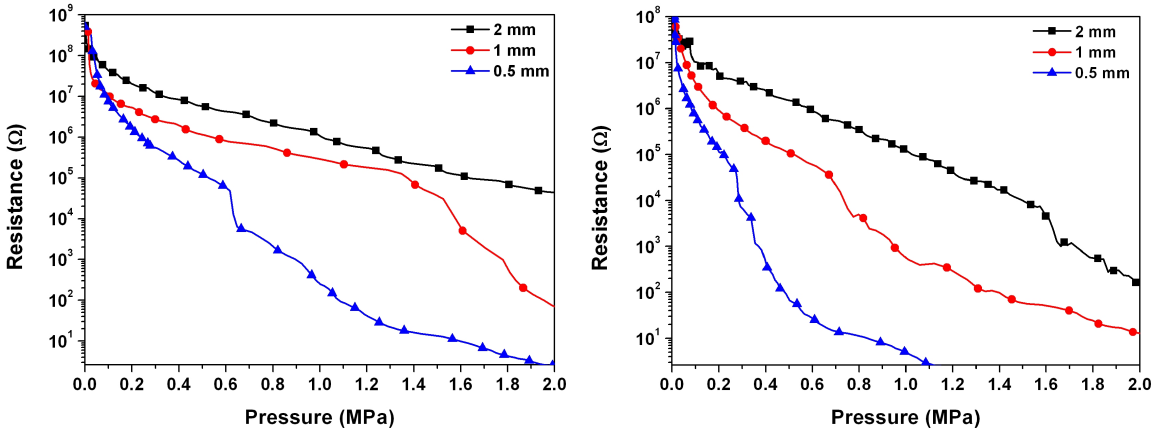

Figure 4.4. Piezoresistive response under compressive pressure as function of sample thickness of PDMS-Cu composites prepared with (a) 200 phr and (b) 250 phr copper content.

Shape and size of the copper-PDMS composite sheet are other fundamental parameters able to affect the piezosensitivity of the sensor. In Fig.4.4 the functional responses of 10x10 mm^2 PDMS-Cu composite samples fabricated with 200 phr and 250 phr composition with different thicknesses (0.5, 1 and 2 mm) are reported. The composite material presented a highly nonlinear relationship between resistance and thickness. The deformation of the samples is in fact strongly dependent on the initial condition of shape, dimension and composition, while the composite resistance in the undeformed state is the same for any thickness. The value of resistance in the undeformed state is the same for all the specimens, while under compression the pressure sensitivity is much higher for thinner samples. To support this statement, the values of piezosensitivity and gauge factor for all these composite samples are reported in Tab.4.2.

4.4 Functional characterization under tensile pressure

Variation of electrical resistance of the material was registered also under the application of a tensile force. For these measurements the composite was prepared in strips 5 mm

Composition	Thickness	Piezosensitivity	Gauge factor
200 phr	0.5 mm	0.0090/kPa	41
200 phr	1 mm	0.0061/kPa	42
200 phr	2 mm	0.0039/kPa	35
250 phr	0.5 mm	0.0173/kPa	36
250 phr	1 mm	0.0109/kPa	48
250 phr	2 mm	0.0059/kPa	38

Table 4.2. Piezosensitivity and gauge factor of the PDMS-Cu composite samples presented in Fig.4.4

wide, 40 mm long and 1 mm thick. When elongated in one direction, the strip of composite contracts in the directions perpendicular to the applied pressure by keeping the volume constant. This would result in a thickening of the interparticle layers in the direction of the applied force and a reduction of the gaps between the particles in the other two directions. Since the copper particles are randomly distributed along the material and are not perfectly aligned on planes, a deformation in the direction perpendicular to the force would mean a redistribution of the particles in the composite that can create tunnelling paths along the samples. Then the resistance of the strip would decreases exponentially with the applied tensile deformation by following the tunnelling conduction mechanism. Evidences of this phenomenon are reported in Fig.4.5(a) where a strip of composite prepared with 250 phr composition was cyclical elongated and then relaxed at different percentages, starting monotonically from 10% up to 40%.

With respect to the PDMS-Ni, the copper-based composite presented an interesting phenomenon during these characterizations. After the first deformation, the following measurements show an enhancement of the electrical resistance circa in correspondence of the end of the previous applied deformation. This behaviour is attributed to the presence of the Mullin effect, a typical phenomenon observed in filled rubbers [7]. Evidence of the Mulling effect was measured also in stress-strain characterization (Fig.4.5(b)) since the mechanical response of the composite strip was dependent on the maximum loading previously encountered.

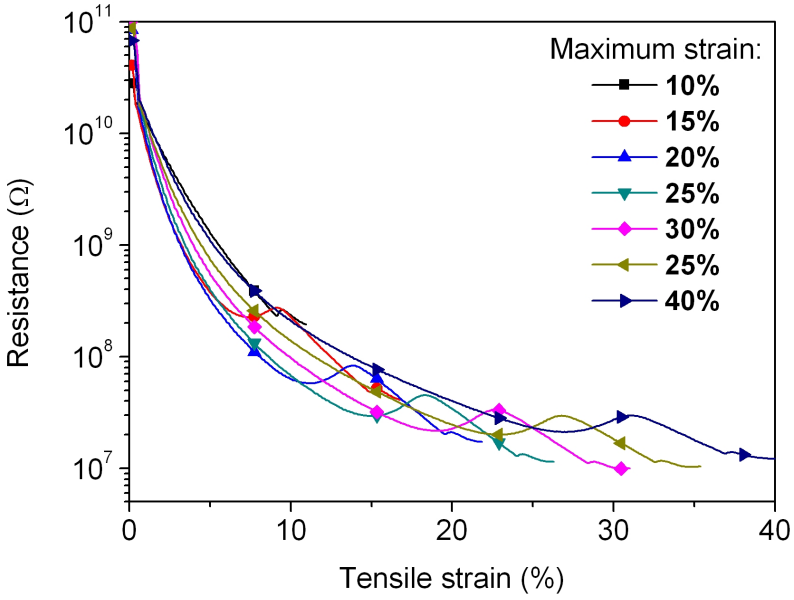

(a)

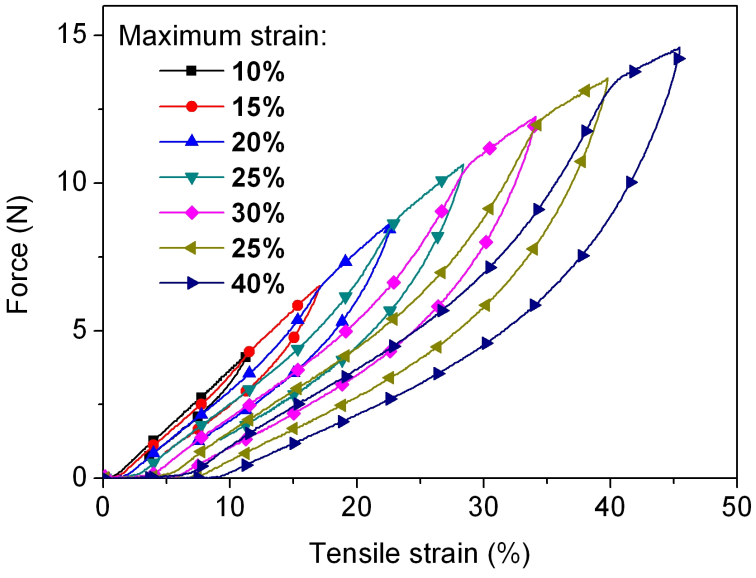

(b)

Figure 4.5. (a) Piezoresistive response under tensile stress and (b) stress-strain diagram of PDMS-Cu composite as function of the maximum elongation.

Bibliography

[1] M. Quaglio, G. Canavese, E. Giuri, S.L. Marasso, D. Perrone, M. Cocuzza, and C.F. Pirri. Evaluation of different PDMS interconnection solutions for silicon, Pyrex and

COC microfluidic chips. *Journal of Micromechanics and Microengineering*, 18(5):055012, 2008.

[2] S.Y. Fu, X.Q. Feng, B. Lauke, and Y.W. Mai. Effects of particle size, particle/matrix interface adhesion and particle loading on mechanical properties of particulate-polymer composites. *Composites Part B: Engineering*, 39(6):933–961, 2008.

[3] F.G. Chang, F. Yang, S.X. Wang, N. Zhang, and G.L. Song. Enhanced piezoresistivity in Niâsilicone rubber composites. *Chinese physics B*, 18(2):652–657, 2009.

[4] J.E. Martin, R.A. Anderson, J. Odinek, D. Adolf, and J. Williamson. Controlling percolation in field-structured particle composites: Observations of giant thermoresistance, piezoresistance, and chemiresistance. *Physical Review B - Condensed Matter and Materials Physics*, 67(9):942071–9420711, 2003.

[5] M.K. Abyaneh and S.K. Kulkarni. Giant piezoresistive response in zinc-polydimethylsiloxane composites under uniaxial pressure. *J. Phys. D: Appl. Phys.*, 41:135405, 2008.

[6] M.K Abyaneh, S Ekar, and S.K. Kulkarni. Piezoresistivity and mechanical behavior of metal-polymer composites under uniaxial pressure. *Journal of Materials Science Research*, 1(3):50–58, 2012.

[7] J. Diani, B. Fayolle, and P. Gilormini. A review on the Mullins effect. *European Polymer Journal*, 45:601–612, 2009.

Chapter 5

Synthesis and integration of spiky nanostructured gold particles as filler of polymeric composites

The use of highly pointed, spiky particles has shown a huge enhancement in electrical conduction in tunnelling piezoresistive composites, since the charges accumulated at the particle protuberances generate a very large electric local field [1]. When the composite material is compressed, the electrons tunnel between the sharp tips at even higher distances with respect to the spherical particles, which results in a larger reduction of the electrical resistance [2, 3].

Indeed, the local charge density enhancement is well known for these highly irregular metal spiky particles, which are widely used for the Surface Enhanced Raman Scattering (SERS) effect [4, 5]. In general, this method allows the detection of single molecules as a result of the enormous amplification of the spectroscopic signals of the molecule upon coupling with nanometer-sized particles [6, 7, 8]. In addition, the size-dependent properties of the nanoparticles can be studied by SERS at the single-particle level.

Recently, much emphasis was put on controlling the shape of the metallic nanoparticles, since the presence of nanosized sharp tips significantly alter the local field enhancement experienced by the adsorbed molecules and thus the SERS efficiency. For this purpose, gold nanostars were recently synthesized and studied as substrate for SERS [9, 10]. Moreover, highly regular shapes of gold nanostars were obtained [11] in a water-free, room-temperature

synthesis assisted by deep-eutectic solvents (DES). DES is an ionic solvent composed of a mixture of quaternary ammonium salts with hydrogen donors, which shows a melting point much lower than those of the individual components [12]. The authors report on the use of choline chloride and urea in a 1:2 molar ratio, respectively, to form a eutectic mixture that is liquid at room temperature [11]. The advantages of DES account for the high viscosity, polarity, thermal stability, ease of preparation and low cost of the products. In addition, DES forms a highly structured "supramolecular" solvent, because of the extended hydrogen-bond network in the liquid state. This feature is convenient to well control the shape of ordered nanoscale structures, such as the aforementioned gold nanostars, without the addition of gold seeds or capping agents.

We modified the experimental parameters for the above synthesis, in order to investigate the most reproducible and feasible reaction conditions for the preparation of highly spiky gold nanoparticles. Indeed, the aim of the performed synthesis was to study the effect of the reactant molar ratio and of the presence of water in the DES solution on particle morphology. In particular, we investigate the relationship between the particle diameter, the protuberance size and shape and the easiest and cost-effective reaction conditions.

Such sharp-pointed nanomaterials find promising application as conductive fillers into polymeric matrices (in this work polydimethylsiloxane, PDMS) for the preparation of piezoresistive composites to be used as strain, pressure, and tactile sensors. Therefore, gold was selected as the conductive filler on the rationale that it has a high conductivity, three times higher than that of nickel and comparable with the copper one, which are the metals normally used in tunnelling conductive composites, and because of the absence of oxidation phenomena [2, 3]. In addition, the nanoscopic size obtained with this synthetic strategy allows the preparation of thin composite films, which can easily be integrated into MEMS (Micro Electro Mechanical System) devices.

In this chapter, we report deep investigation on the nanoparticles producted with the DES syntheses and the preparation and characterization of a composite based on the synthesized gold nanostars that show the most appropriate features in terms of tip morphology and overall particle size, which thus demonstrate their efficacy as filler for tunneling conductive polymer composites.

5.1 Experimental Section

All chemicals, with the exception of polydimethylsiloxane (PDMS), were obtained from Sigma Aldrich and used as received without any further purification. The bicomponent PDMS was obtained from Dow Corning Corporation (SYLGARD 184). The deep eutectic solvent (DES) was prepared by combining urea (purity $\geq$ 99.5%) and choline chloride (ChCl, $\geq$ 98%) at a molar ratio of 2:1. The two compounds were mixed at 100°C until a homogeneous colorless liquid solution was formed. The resulting mixture was then cooled down at room temperature.

For the gold nanostars synthesis in the presence of water, the DES was mixed with doubly distilled water (from Millipore Direct-Q System) at a volume ratio of 1:1. Hydrogen tetrachloroaurate trihydrate ($HAuCl_4 \cdot 3H_2O$, 0.058 g, metal basis 99.99%) was dissolved in DES (25 mL) or in the DES/water mixture (25 mL) and a dark yellow solution was obtained. Separately, a second solution of DES (or DES/water) (25 mL) and L-ascorbic acid (AA, 0.104, 0.156, 0.234, or 0.312 g) was prepared, with a final AA/HAuCl4 molar ratio of 4:1, 6:1, 9:1, or 12:1, respectively). The second solution was then added to the first to give a pale yellow mixture. The reaction time to completion was about 4 h with magnetic stirring at room temperature. The precipitate product was then centrifuged at 5500 rpm (2875 RCF) for 20 min and dispersed in doubly distilled water. This procedure was repeated three times.

For the preparation of the PDMS+DES-6 composite, the gold nanostars were dispersed in ethanol, and the PDMS copolymer was then added to the solution at a weight ratio of 1:1 (100 phr). The blend was mixed in an ultrasound bath at 70°C until all the ethanol was evaporated. The PDMS curing agent was then added with a weight ratio of 1:10 with respect to the co-polymer. The resulting paste was outgassed for 1 h under vacuum at room temperature, in order to avoid the formation of air bubbles and to eliminate the last traces of ethanol. Therefore, the composite mixture was poured in polymethylmethacrylate (PMMA) moulds and thermally cured in an oven at 75°C for 10 h.

The morphological characterization and the energy-dispersive Xray spectroscopy of the gold nanostars were carried out by field emission scanning electron microscopy (FESEM, Zeiss SupraTM 40), equipped with a INCA Oxford Energy Dispersive X-ray (EDX) Spectroscopy detector. The X-ray diffraction patterns were obtained on a X'Pert Philips with Cu-K_α radiation at λ = 1.5418 Å. The electro-mechanical characterization was performed

Sample	Water content (%vol)	AA:$HAuCl_4$ molar ratio	D_{core} (nm)[a]	H_t (nm)[b]	B_t (nm)[c]	C_s (nm)[d]
DES-4	0 (Dry)	4:1	0	416	82	46.7
DES-6	0 (Dry)	6:1	350	146	172	44.3
DES-9	0 (Dry)	9:1	521	396	666	38.2
DES-12	0 (Dry)	12:1	709	555	331	35.1
DES-H_20-4	50	4:1	232	121	173	36.6
DES-H_20-6	50	6:1	314	112	227	31.2
DES-H_20-9	50	9:1	395	97	154	42.1
DES-H_20-12	50	12:1	433	37	10	34.9

[a] average diameter of the inner spherical core of the nanostar
[b] average height of the tip
[c] average lateral size of the tip at the base
[d] crystal size calculated from the Debye-Scherrer equation

Table 5.1. Summary of the prepared samples by varying the reactant molar ratio (AA:$HAuCl_4$) and the water content. The resulting morphological and structural features of the gold nanostars with special attention to the protuberances and crystal sizes are also reported.

with a piezoelectric evaluation system (aixPES) supplied by aixACCT Systems GmbH, which is able to measure currents in the picoampere range. The samples were placed in a customized sample holder with the possibility of applying static uniaxial forces of up to 5 kN.

5.2 Synthesis results

The synthesis of gold nanostars was carried out by mild reduction of gold ($HAuCl_4 \cdot 3H_2O$) with L-ascorbic acid (AA) in the presence of DES, prepared from choline chloride and urea in a 1:2 mixture. In particular, the final morphology of the obtained gold nanostars was studied by variation of the reactant molar ratio, i.e. AA to gold source and by substitution of 50% (vol) of the total DES volume with water, see Tab.5.1.

Under dry conditions, the obtained gold particles show sharp tips, as reported in Fig.5.1 from FESEM imaging. Tab.5.1 also reports on the size of the nanoparticles inner core (D_{core}), the height (H_t), and length at the base (B_t) of their protuberances, as an average from measuring 50 particles per sample. By increasing the molar ratio of AA: $HAuCl_4$, the number, the height (H_t), and the length at the base (B_t) of the tips increases, to form

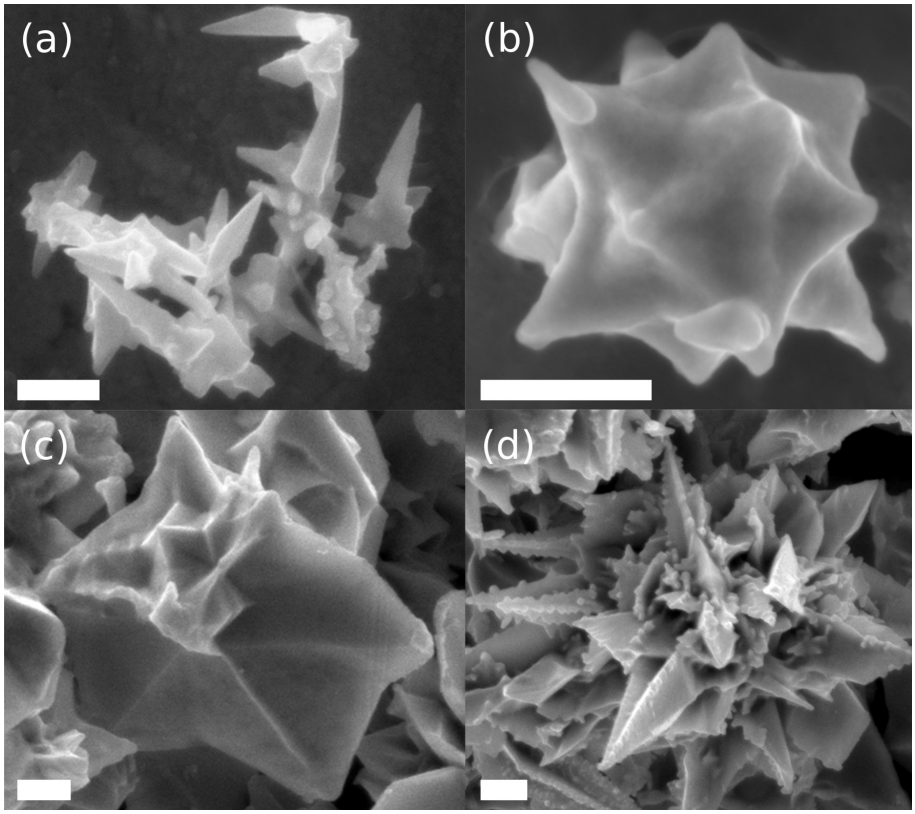

Figure 5.1. Nanosized gold spiky particles, synthesized under dry conditions by using an L-ascorbic acid (AA)/hydrogen tetrachloroaurate ($HAuCl_4$) ratio of (a) 4:1, (b) 6:1, (c) 9:1, (d) 12:1. The scale bar is 200 nm.

highly multibranched gold nanostars, as shown in Fig.5.1(d). Liao et al. [11] also observed the formation of similar nanothorns by adjusting the content of water to higher than 10000 ppm. In our synthesis, indeed, we worked under dry conditions without monitoring the amount of humidity in the synthetic batch, thus we could assume that all the processes presented here performed under "dry conditions" should contain traces of water related to the humidity of the air. However, we elaborate on the rationale of this choice, since we want to study the most reliable and cost-effective process for the further development of piezoresistive composite materials to be used as strain or pressure sensors.

In addition, the core size (D_{core}) of the gold spiky particles also increases, starting from single sharp pyramids for the lower AA:$HAuCl_4$ ratio (where D_{core}=0 for sample DES-4, Fig.5.1(a)) to bulkier core sizes (D_{core}=709 nm in the case of sample DES-12, Fig.5.1(d)). A trend for this behaviour can be extrapolated by calculating the ratio between the core size

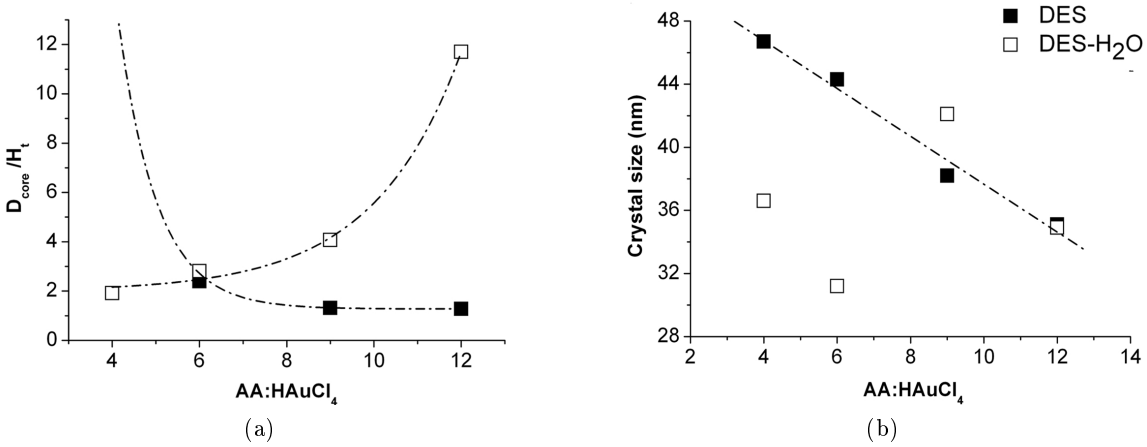

Figure 5.2. (a) The average core size (D_{core}) to tip height (H_t) ratios of the gold nanoparticles synthesized by both synthetic routes are plotted vs. the reactant molar ratio (AA:$HAuCl_4$) and fitted with an exponential model; (b) The average crystal size of the gold nanoparticles calculated by the Debye-Scherrer model vs. the AA:$HAuCl_4$ molar ratio. Only the data related to the synthesis under dry conditions are fitted linearly. Filled squares: samples prepared under dry conditions; empty squares: samples prepared in the presence of 50% (vol) water and 50% (vol) DES.

of the gold nanoparticles and their tip height, D_{core}/H_t. By plotting these values vs. the AA:$HAuCl_4$ molar ratio (Fig.5.2(a), filled squares), one can clearly observe an exponential decay behaviour of the ratio D_{core}/H_t with respect to the reactant molar ratio, as confirmed by the good fit with a mathematical model (dash-dotted line in Fig.5.2(b), see section 5.3 for further details).

Energy-dispersive X-ray spectroscopy (EDS) indicates that all the synthesized nanoparticles are composed of only gold (Fig.5.3(a)) with a face-centered cubic (fcc) structure, as indexed by the X-ray diffraction patterns reported in Fig.5.3(b).

The crystal sizes of the gold nanostars were calculated by the Debye-Scherrer model applied to the XRD spectra of Fig.5.3 and are reported in Tab.5.1. The obtained values for the dry syntheses show that the gold crystal size reduces almost linearly upon increase in the AA:$HAuCl_4$ molar ratio. This trend is shown in Fig.5.2(b) (filled squares) and was fitted with a linear equation (see section 5.3 for further details). Since the crystal size of the nanoparticles is smaller than the dimensions of the particles reported in Tab.5.1, i.e. D_{core}, H_t and B_t, the gold nanostars should be polycrystalline.

According to the obtained trends, some assumptions can be tentatively drawn on the

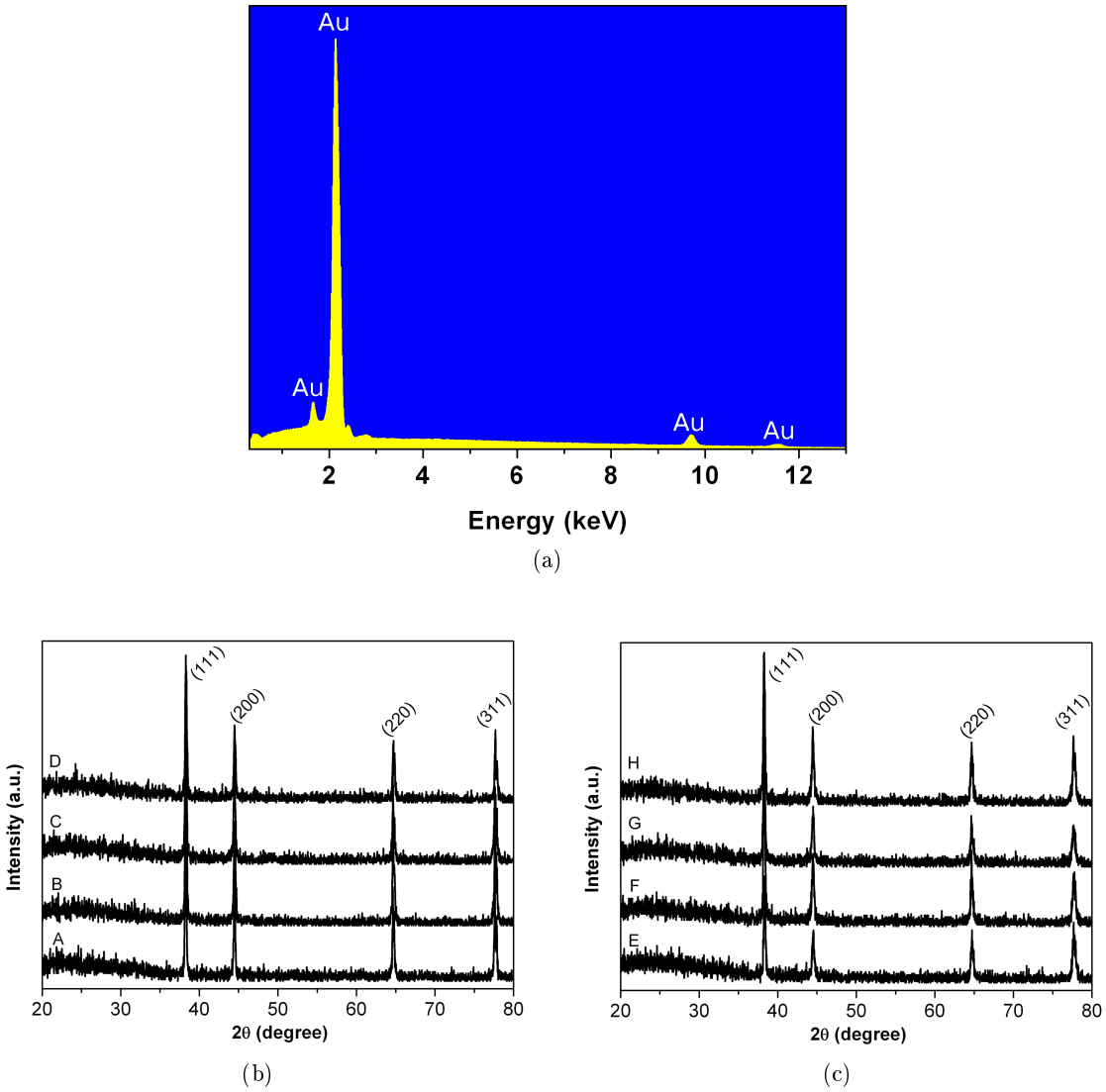

Figure 5.3. Energy-dispersive X-ray spectroscopy (EDS) was carried out on all samples, showing that the nanoparticles are constituted only of gold. (a) representatively shows only the result obtained for sample DES-6. X-ray diffraction (XRD) patterns of spiky gold nanoparticles synthesized (a) under dry conditions or (b) in the presence of 50(vol) of water. A: DES-4; B: DES-6; C: DES-9; D: DES-12; E: DES-H_2O-4; F: DES-H_2O-6; G: DES-H_2O-9; H: DES-H_2O-12.

formation mechanism of the gold nanostars under dry conditions. The star-shaped gold nanoparticles are the result of the mild reduction of $HAuCl_4$ by L-ascorbic acid at room temperature in the DES. Several authors reported that the main role of the DES in the synthesis is as liquid template [13] and as particle stabilizer [11]. It was also previously

shown [14, 15] that an excess of L-ascorbic acid promotes the anisotropic growth, which thus produces particles with a branched shape. It seems also that upon increasing the molar ratio of L-ascorbic acid to gold source, the reduction efficiency is higher, which thus increases the nucleation rate of gold to form several crystal domains with a smaller size, as evidenced by the increase in the number of protuberances. The final polycrystalline structure of the gold spiky particles is the result of subunit growth and aggregation of several small crystal domains.

By substituting half of the DES volume with water in the synthetic batch, particles with a more pronounced spherical shape are obtained. This effect is even more evident upon increasing the L-ascorbic acid to gold source molar ratio (Fig.5.4). Under these synthetic conditions, the core size of the gold particles increases, but not as much as in the previous synthesis batches with only DES as solvent (see Tab.5.1). In addition, as the molar ratio of the reactants increases, the height (H_t) and the length at the base (B_t) of the tips at the gold surface strongly decrease (Tab.5.1). As also observed under dry conditions, the number of the protuberances also increases because of excess of L-ascorbic acid. Interestingly, with a ratio AA/$HAuCl_4$ of 12:1, meatball gold nanoparticles of about 500 nm in diameter are obtained with a rough surface. According to previous considerations, several small tips (H_t=37 nm, B_t=10 nm) are present at the core surface (Fig.5.4(d)), and it seems that their growth in height and lateral size is completely prevented. The particle morphology trend can be summarized in Fig.5.2(a) (empty squares); the D_{core}/H_t ratio grows exponentially by increasing the AA:$HAuCl_4$ molar ratio.

In contrast to the previous syntheses under dry conditions, the crystal sizes do not follow a trend by varying the molar ratio of the reactants (Tab.5.1). Polycrystalline face centered cubic (fcc) gold nanoparticles were also obtained in this case (Fig.5.3(c)) and are constituted only of gold. As already discussed for the synthesis under dry conditions, by increasing the molar ratio of AA to gold source, several crystal domains with a smaller size are formed. Therefore, the number of protuberances at the particle core increases. This is attributed to a higher nucleation rate of gold. However, it is also assumed that the presence of water inhibits the effect of L-ascorbic acid in inducing anisotropic crystal growth. This therefore results in a homogeneous growth of the gold nanoparticles, which leads to more spherical shapes. Wang and Halas proposed that the nucleation sites grow into nanoscale primary particles by diffusion capture of the remaining atoms [16]. These primary particles then form aggregates, under appropriate reaction conditions, which leads to the formation

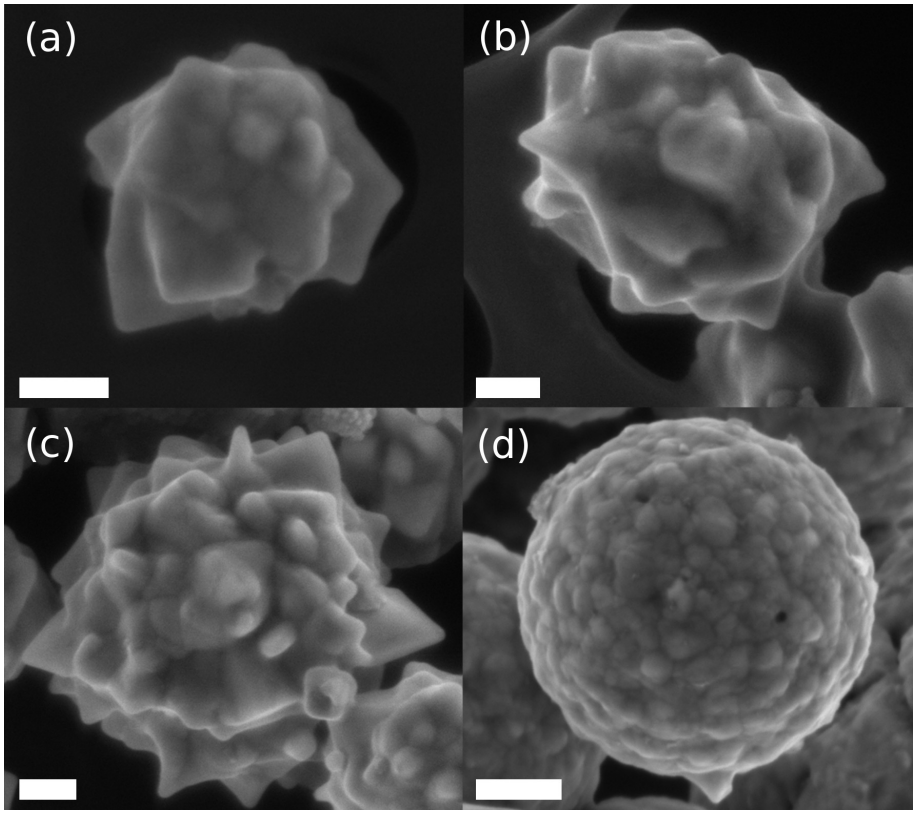

Figure 5.4. Nanosized gold spiky particles, synthesized in the presence of water [50% (vol) H_2, 50% (vol) DES] by using an L-ascorbic acid (AA)/hydrogen tetrachloroaurate ($HAuCl_4$) ratio of (a) 4:1, (b) 6:1, (c) 9:1, (d) 12:1. The scale bar is 100 nm.

of larger spherical aggregates with nanoscale surface roughness.

5.3 Mathematical model of particles growth

The ratio between the core diameter (D_{core}) and the protuberances height (H_t) of the synthesized gold nanoparticles was plotted versus the L-Ascorbic Acid to gold precursor (AA:$HAuCl_4$) molar ratio in order to establish a trend, as shown in Fig.5.2.

It was found that the values of D_{core}/H_t can be fitted with an exponential equation (5.1):

$$\frac{D_{core}}{H_t} = \left(\frac{D_{core}}{H_t}\right)_0 + A\ e^{kx} \tag{5.1}$$

where x is the AA:$HAuCl_4$ molar ratio, $(D_{core}/H_t)_0$ is the asymptotic value, A is the exponential coefficient and k the growth rate.

The calculated parameters are repoted in Tab.5.2, where R^2 and χ^2 are parameters to evaluate the goodness of the fit.

	$(D_{core}/H_t)_0$	A	k	R^2	χ^2
100 %vol DES (dry condition)	1.276 ±0.007	1251 ±41.583	-1.128 ±0.003	0.998	$8.428 \cdot 10^{-5}$
50 %vol DES – 50 %vol H_2O	1.981 ±0.458	0.025 ±0.030	0.497 ±0.099	0.991	0.178

Table 5.2. Fitting parameters obtained by applying the exponential equation to the graph in Fig.5.2(a) of the main text.

It is noteworthy that the equation (5.1) describes an exponential decay of the D_{core}/H_t value by increasing the reactant molar ratio in the case of gold nanoparticles synthesized in dry conditions (k = -1.128). In contrast, an exponential growth well describes the behaviour of D_{core}/H_t when the synthesis is carried out in the presence of water.

Concerning the variation of the crystal size versus the AA:$HAuCl_4$ molar ratio, it was found that the trend is well fitted by a linear regression (5.2) only in the case of dry condition synthesis:

$$C_{size} = A + Bx \tag{5.2}$$

where the fitting parameters are indicated in Tab.5.3, while in the case of presence of water the crystal size values are completely random.

	A	B	R^2
100 %vol DES (dry condition)	52,826 ±1,193	-1,516 ±0,143	0,99118

Table 5.3. Fitting parameters obtained by applying the linear regression to the crystal size variation versus the reactant molar ratio, as reported in the graph of Fig.5.2(b) (filled squares) of the main text.

5.4 Composite preparation and characterization

In order to prove that the morphology of the synthesized gold nanostars is very well suited for the use as filler in piezoresistive composites, the gold nanoparticles were dispersed in polydimethylsiloxane (PDMS) with a weight ratio of 1:1 (inset of Fig.5.5). In particular, the most suitable sample among the above syntheses for the preparation of the composite was DES-6, because of its small dimension, spiky shape, and number of tips.

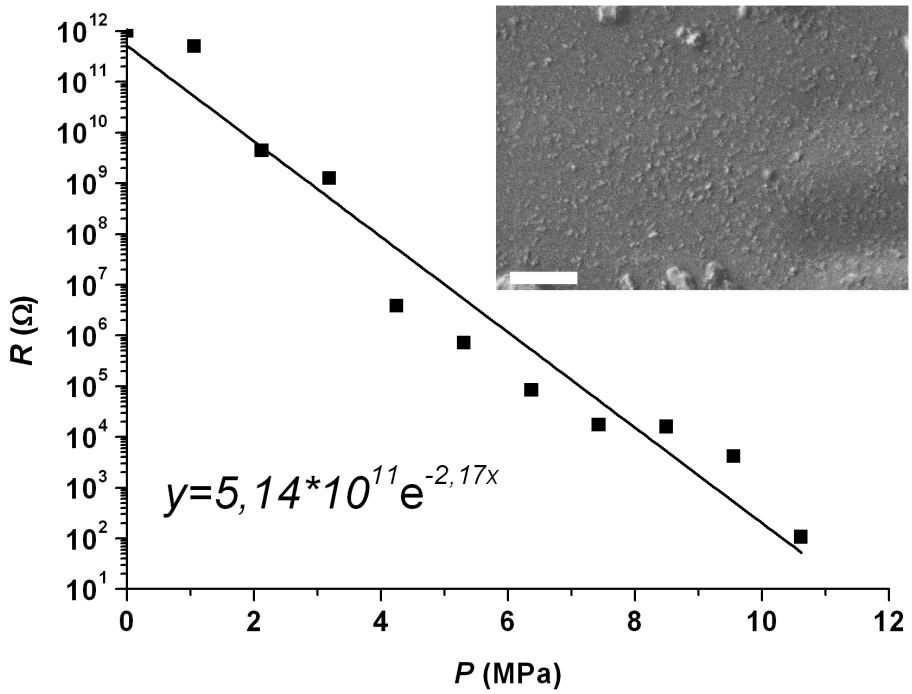

Figure 5.5. Electrical resistance of the PDMS+DES-6 composite as a function of uniaxial pressure and its exponential fitting. In the inset, the FESEM image of the PDMS+DES-6 composite is shown. The scale bar is 10 μm.

The prepared composite, with a thickness of 100 μm, was tested under different mechanical pressures to evaluate the electric resistance (Fig.5.5). The composite (PDMS+DES-6) exhibits a variation of up to ten orders of magnitude in the resistance under a uniaxial pressure of 10 MPa, and therefore passes from a highly insulating state to a conductive one. The experimental points collected during the measurements were fitted with an exponential trend:

$$R(\Omega) = 5.14 \cdot 10^{11} \exp(-2.17 P(MPa)) \tag{5.3}$$

which confirms that the conduction mechanism in the metal-polymer composite could be attributed to a quantum tunnelling mechanism. The final pressure applied to the sample reaches high values, thus further optimization of the composition and filler amount in the PDMS matrix should be carried out. However, these results confirm that, as proof of principle, the gold nanostars, synthesized with the method presented above, can be a suitable solution as filler for piezoresistive composites. Their spiky morphology and sub-micrometer size allows their further integration in MEMS technology for promising developments of strain, pressure, and tactile sensors, as confirmed by the results obtained from the prepared PDMS-gold composite.

Bibliography

[1] C.J. Edgcombe and U. Valdrè. Microscopy and computational modelling to elucidate the enhancement factor for field electron emitters. *Journal of Microscopy*, 203:188–194, 2001.

[2] D. Bloor, K. Donnelly, P. J Hands, P. Laughlin, and D. Lussey. A metal-polymer composite with unusual properties. *J. Phys. D: Appl. Phys.*, 38:2851–2860, 2005.

[3] S. Stassi, V. Cauda, G. Canavese, D. Manfredi, and C.F. Pirri. Synthesis and characterization of gold nanostars as filler of tunneling conductive polymer composites. *European Journal of Inorganic Chemistry*, 16:2669–2673, 2012.

[4] E. Nalbant Esenturk and A.R. Hight Walker. Surface-enhanced raman scattering spectroscopy via gold nanostars. *Journal of Raman Spectroscopy*, 40(1):86–91, 2009.

[5] X.S. Shen, G.Z. Wang, X. Hong, and W. Zhu. Nanospheres of silver nanoparticles: Agglomeration, surface morphology control and application as SERS substrates. *Physical Chemistry Chemical Physics*, 11(34):7450–7454, 2009.

[6] S. Nie and S.R. Emory. Probing single molecules and single nanoparticles by surface-enhanced raman scattering. *Science*, 275(5303):1102–1106, 1997.

[7] R.A. Alvarez-Puebla, A. Agarwal, P. Manna, B.P. Khanal, P. Aldeanueva-Potel, E. Carbó-Argibay, N. Pazos-Pérez, L. Vigderman, E.R. Zubarev, N.A. Kotov, and L.M. Liz-Marzán. Gold nanorods 3D-supercrystals as surface enhanced raman scattering spectroscopy substrates for the rapid detection of scrambled prions. *Proceedings of*

the National Academy of Sciences of the United States of America, 108(20):8157–8161, 2011.

[8] K. Critchley, B.P. Khanal, M.L. Górzny, L. Vigderman, S.D. Evans, E.R. Zubarev, and N.A. Kotov. Near-bulk conductivity of gold nanowires as nanoscale interconnects and the role of atomically smooth interface. *Advanced Materials*, 22(21):2338–2342, 2010.

[9] C.G. Khoury and T. Vo-Dinh. Gold nanostars for surface-enhanced raman scattering: Synthesis, characterization and optimization. *J. Phys. Chem. C*, 112:18849–18859, 2008.

[10] P.S. Kumar, I. Pastoriza-Santos, B. Rodriguez-Gonzalez, F. Javier. Garcia de Abajo, and L.M. Liz-Marzan. High-yield synthesis and optical response of gold nanostars. *Nanotechnology*, 19:015606, 2008.

[11] H.G. Liao, Y.X. Jiang, Z.Y. Zhou, S.P. Chen, and S.G. Sun. Shape-controlled synthesis of gold nanoparticles in deep eutectic solvents for studies of structure-functionality relationships in electrocatalysis. *Angewandte Chemie (International ed. in English)*, 47(47):9100–3, 2008.

[12] H.G. Morrison, C.C. Sun, and S. Neervannan. Characterization of thermal behavior of deep eutectic solvents and their potential as drug solubilization vehicles. *International Journal of Pharmaceutics*, 378(1-2):136–139, 2009.

[13] E.R. Parnham, E.A. Drylie, P.S. Wheatley, A.M.Z. Slawin, and R.E. Morris. Ionothermal materials synthesis using unstable deep-eutectic solvents as template-delivery agents. *Angewandte Chemie - International Edition*, 45(30):4962–4966, 2006.

[14] J.L. Burt, J.L. Elechiguerra, J. Reyes-Gasga, J.M. Montejano-Carrizales, and M. Jose-Yacaman. Beyond archimedean solids: Star polyhedral gold nanocrystals. *Journal of Crystal Growth*, 285:681–691, 2005.

[15] C.-H. Kuo and M.H. Huang. Synthesis of branched gold nanocrystals by a seeding growth approach. *Langmuir*, 21(5):2012–2016, 2005.

[16] H. Wang and N.J. Halas. Mesoscopic Au "meatball" particles. *Advanced Materials*, 20(4):820–825, 2008.

Chapter 6

Evaluation of the conductive nanostructured particles as filler in tunnelling piezoresistive composites

The properties of piezoresistive composite materials could be tuned by varying the nature and the morphology of the particles, used as functional filler, and the type of matrix [1, 2]. By varying the type and amount of fillers, the composite can assume the electrical properties of an insulator up to those of a good conductor. In the piezoresistive composites based on tunnelling conduction mechanism, a small variation of the external load induces a huge change of the electrical conductivity [3, 4, 5]. Without any mechanical deformation upon an applied bias, the prepared composites present an insulating electric behaviour, while, when subjected to mechanical load, the polymer thickness reduces, thus decreasing the tunnelling barrier. As a consequence, the probability of tunnelling phenomena increases, resulting in a exponential reduction of the bulk electrical resistance. In these composites, the shape and dimension of the filler particles become as important as the filler nature and amount. In particular, the composites prepared with conductive particles presenting sharp and nanostructured tips on the surface exhibit a huge variation of the electrical conduction in response to a mechanical strain.

This chapter presents a comparison between three piezoresistive composite materials, based on nanostructured conductive fillers in a polydimethylsiloxane insulating elastomeric

matrix, shown in the previous chapters. Three different metal fillers were tested: commercial nickel (chapter 3) and copper spiky-particles (chapter 4) and synthesized highly pointed gold nanostars (chapter 5). These particles were chosen because of their high electrical conductivity and especially for the presence of nanosized sharp tips on their surface. These features generate an enhancement of the local electric field increasing the tunnelling probability between the particles [6]. Different figures of merit concerning the morphology of the fillers were evaluated and correlated with the corresponding functional response of the composite. The aim is to understand how the morphological features of the nanostructured particles influence the minimum and the maximum required amount of the fillers to obtain similar piezoresistive performances among the different composites. In this way, it could be possible to select the best filler and to easily tune the functional properties of the composites in order to reach the required sensor sensitivity.

6.1 Methods of analysis

The nickel powder used in this work was supplied by Vale Inco Ltd. (type 123), copper was obtained from Pometon (LT10) and the bi-component polydimethylsiloxane (PDMS) was purchased by Dow Corning Corporation (SYLGARD 184). For the synthesis of the gold nanoparticles, all the chemicals were obtained from Sigma Aldrich and used as received without any further purification. The synthetic procedure to synthesize shape-controlled, highly pointed, and nanometric-sized gold nanostars and to prepare nickel, copper and gold based PDMS composite are presented in the previous chapters (3, 4 and 5). All the compared samples had a footprint of 10*10 mm^2 and the thickness of 1 mm. The resistance of the nickel and copper composites was circa 1 GΩ, in the absence of an applied pressure, while for the gold composite was around 100 GΩ. The morphological characterization was carried out by a field emission scanning electron microscope (FESEM). For each metal filler, circa 100 particle tips where measured from the FESEM images in term of radius of curvature (R_t) and aspect ratio between the tip height (H_t) and its full width at half maximum (FWHM). In order to evaluate the sharpness of the spiky particles, the ratio between the H_t and the core particle diameter (D_{core}) were also calculated.

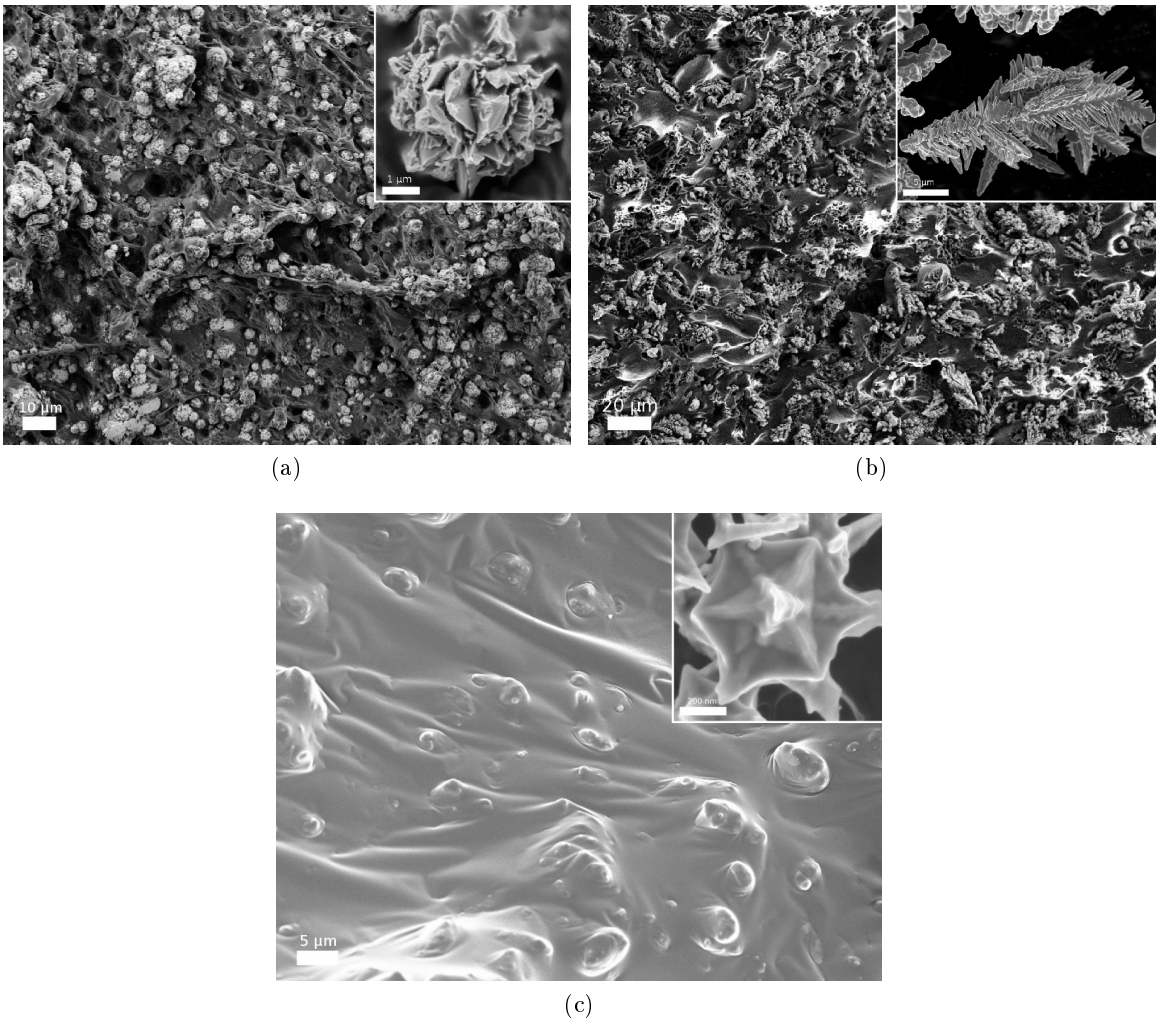

(a) (b)

(c)

Figure 6.1. Scanning electron microscopy images of different PDMS-metal composites and of nanoshaped-spiky particles in the insets, at different magnifications. (a) Nickel, (b) copper, and (c) gold.

6.2 Comparison between the three piezoresistive composite

Here the piezoresistive performances of three metal conductive composites, with different fillers, i.e., nickel, copper, and gold are compared. The results are presented in terms of electric resistance variation as a function of the applied mechanical pressure, obtained for the optimized compositions of the final composites.

In the previous chapters, we tried indeed different weight ratios between the filler

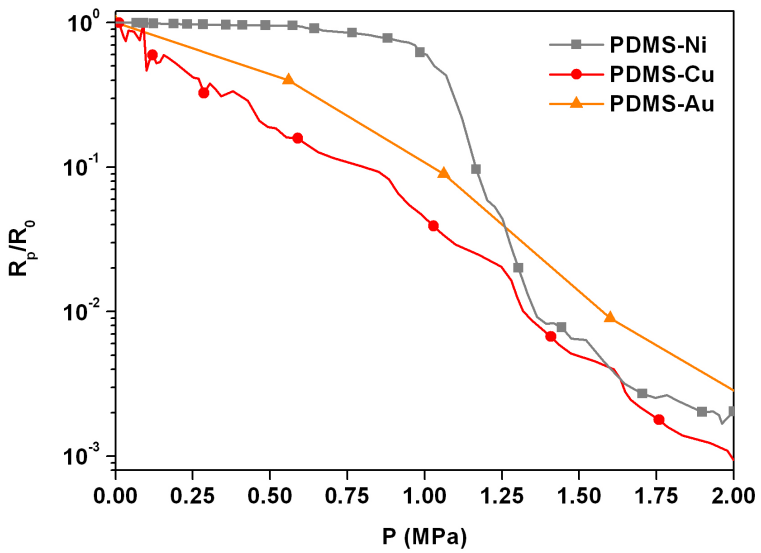

Figure 6.2. Electric resistance variation of the piezoresistive composites (with minimum filler amount) as a function of the applied uniaxial pressure.

amount and the polymeric matrix, ranging from 100 phr to 550 phr. In Fig.6.1, we identify the minimum weight amount per each kind of filler, required to obtain an appreciable and comparable tunnelling conduction effect between the different composites. Therefore, comparable electric resistance variations as a function of the applied mechanical pressure (Fig.6.2) were obtained with a metal content of 300 phr for the PDMS-Ni, 175 phr for PDMS-Cu, and 100 phr for the PDMS-Au composites (see also Tab.6.1). In contrast, lower filler to polymer ratios with respect to the previously indicated ones showed an insulating behaviour.

In order to evaluate the strain sensitivity of the composites, we calculated the gauge factor with the method reported in the work of Abyaneh and Kulkarni [5]. We obtained the values of approximately 18 for the nickel-based composite, and about 10 for the copper and gold ones. These gauge factors could be increased by enhancing the content of metallic filler in the polymeric matrix.

The three selected particles have different size and shape, ranging from spiky micrometric sized nickel particles (average diameter, 4.5 μm, Fig.6.1(a)), to elongated multi-branched copper ones (average diameter, 12 μm, Fig.6.1(b)) up to gold nanosized stars (average diameter, 450 nm, Fig.6.1(c)). It was already reported in the literature [3] that highly pronounced and elongated tips at the particle surface increase the electric conductance throughout the

Metal particles	R_t[a][nm]	H_t/FWHM[b]	H_t/D_{core}[c]	Metal content
Ni	43	1.1	0.09	300 phr
Cu	975	3.6	0.37	175 phr
Au	17	2.3	0.34	100 phr

[a] average tip radius
[b] aspect ratio between the H_t and FWHM
[c] ratio between the H_t and D_{core}

Table 6.1. Figures of merit of the nanoshaped-spiky fillers

composite, amplifying the electric field and, thus, the tunnelling probability among the spiky fillers. It is therefore clear that the lower the curvature radius of the conductive tips, the higher the tunnelling conductance effect in the composite.

Based on these FESEM images, we have therefore calculated the different figures of merit describing the morphological features of our spiky particles (see Tab.6.1), as also schematically reported for clarity in Fig.6.3. Both nickel and gold show nanostructured tips with a small R_t (43 and 17 nm, respectively). However, in the case of nickel, the tips are quite short with respect to the particle micrometric size, thus the H_t/D_{core} ratio results very low (0.09). In contrast, very similar H_t/D_{core} ratio are obtained for both copper and gold spiky-particles (0.37 and 0.34, respectively).

Considering the obtained values of electric resistance, one can observe a strong relationship between the morphological data calculated here and the used filler amount in the final composite. First, the copper and gold-based composites have both shown remarkable tunnelling conduction values at lower filler amount (175 phr for PDMS-Cu and 100 for PDMS-Au) with respect to the weight ratio used for the nickel-based composite (300 phr). We attribute this effect to the higher H_t/D_{core} ratio obtained for both copper and gold with respect to the nickel one.

Additionally, another morphological parameter was calculated, that is the aspect ratio between the H_t and its FWHM. Higher is this value, sharper and more slender is the tip. We note that both copper and gold fillers have a higher H_t/FWHM ratio than the nickel one.

The combination of both parameters, i.e., high H_t/FWHM and H_t/D_{core} ratios, implies the presence of sharp tips showing a pronounced height with respect to the core size of the particles. This means that a lower amount of material in weight is required for obtaining

similar conductance values, since the probability of the tip to form a tunnelling conduction is higher with respect to massive, spherical shaped nanoparticles with the same size.

In addition, the gold-based composite requires an even lower filler amount (100 phr) than the copper one (175 phr) to obtain similar tunnelling conductance values. We note, however, that the H_t/D_{core} ratio of gold is slightly smaller (0.34) than those of copper (0.37) as well as the H_t/FWHM ratios (2.3 for gold versus 3.6 for copper). Thus, the lower radius of curvature of the gold tip shows to play here a predominant role in the tunnelling conduction enhancement. Indeed, the R_t of gold is about 60 times smaller than that of copper. It is therefore clear that, in the case of gold, the presence of either high H_t/D_{core} and H_t/FWHM ratios and small R_t is a fundamental prerequisite for obtaining high tunnelling conductance value with a low filler to polymer weight ratio.

On the contrary one can also compare the functional response of the composite as function of the highest metal loading reached. In this perspective, the use of gold as filler becomes not anymore favorable. In Fig.6.4 the piezoresistive characteristics were obtained with a metal content of 500 phr for the PDMS-Ni (the 550 phr composite was too difficult to process and for this reason was not considered in this analysis), 250 phr for PDMS-Cu, and 100 phr for the PDMS-Au composites. Gold based composites were prepared only with the 100 phr composition because of the cost of the material, the time of synthesis and above

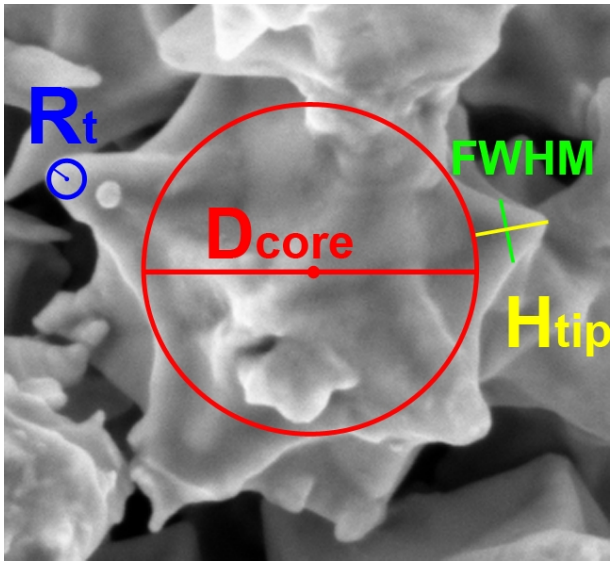

Figure 6.3. The scheme of the geometric parameters reported in Tab.6.1